EUROGRAPHICS 2005 / M. Alexa and J. Marks
(Guest Editors)

Volume 24 (*2005*), *Number 3*

Structure Preserving CAD Model Repair

Stephan Bischoff Leif Kobbelt

Computer Graphics Group
RWTH Aachen

Abstract

There are two major approaches for converting a tessellated CAD model that contains inconsistencies like cracks or intersections into a manifold and closed triangle mesh. Surface oriented algorithms try to fix the inconsistencies by perturbing the input only slightly, but they often cannot handle special cases. Volumetric algorithms on the other hand produce guaranteed manifold meshes but mostly destroy the structure of the input tessellation due to global resampling. In this paper we combine the advantages of both approaches: We exploit the topological simplicity of a voxel grid to reconstruct a cleaned up surface in the vicinity of intersections and cracks, but keep the input tessellation in regions that are away from these inconsistencies. We are thus able to preserve any characteristic structure (i.e. iso-parameter or curvature lines) that might be present in the input tessellation. Our algorithm closes gaps up to a user-defined maximum diameter, resolves intersections, handles incompatible patch orientations and produces a feature-sensitive, manifold output that stays within a prescribed error-tolerance to the input model.

Categories and Subject Descriptors (according to ACM CCS): I.3.5 [Computational Geometry and Object Modeling]: Curve, surface, solid, and object representations

1. Introduction

A common dilemma in todays CAM production environments are the different geometry representations that are employed by CAD systems on the one hand and downstream applications on the other hand. While CAD systems usually represent a model by a set of trimmed NURBS patches or by other surface primitives (that possibly are extracted from a CSG representation), downstream applications like computational fluid- or structure simulation, rapid prototyping, and numerically controlled machining rely on closed and consistent manifold triangle meshes as input. The conversion from one representation into the other is not only a major bottleneck in terms of time, but also with respect to the accuracy and quality of the output and thus directly impacts all subsequent production stages.

Common tessellation algorithms are able to efficiently and accurately convert *single* surface primitives into triangle meshes, but usually cannot handle continuity constraints between different primitives or detect and resolve intersecting geometry. This leads to artifacts like gaps, overlaps, intersections, or inconsistent orientations between the tessellated patches, which often have to be repaired in a manual and tedious postprocessing step. For this reason, quite some effort has been put into algorithms that are able to automatically repair such models.

There are two major approaches for converting a tessellated CAD model that contains inconsistencies like gaps or intersections into a clean and manifold closed triangle mesh. *Surface oriented algorithms* try to explicitly compute or identify consistent (sub-)patches that are subsequently stitched together by snapping boundary elements. These algorithms only minimally perturb the input patches, but due to numerical issues cannot guarantee a consistent output mesh and hence usually require user-interaction. *Volumetric algorithms* on the other hand use a signed distance grid as an intermediate representation and are able to produce guaranteed manifold reconstructions. Unfortunately, these algorithms destroy the structure of the input tessellation due to a global resampling stage. Furthermore the resolution of the underlying grid limits the quality of the reconstruction.

In this paper we combine the advantages of both approaches: We exploit the topological simplicity of a voxel grid to reconstruct a cleaned up surface in the vicinity of intersections and cracks, but keep the input tessellation in

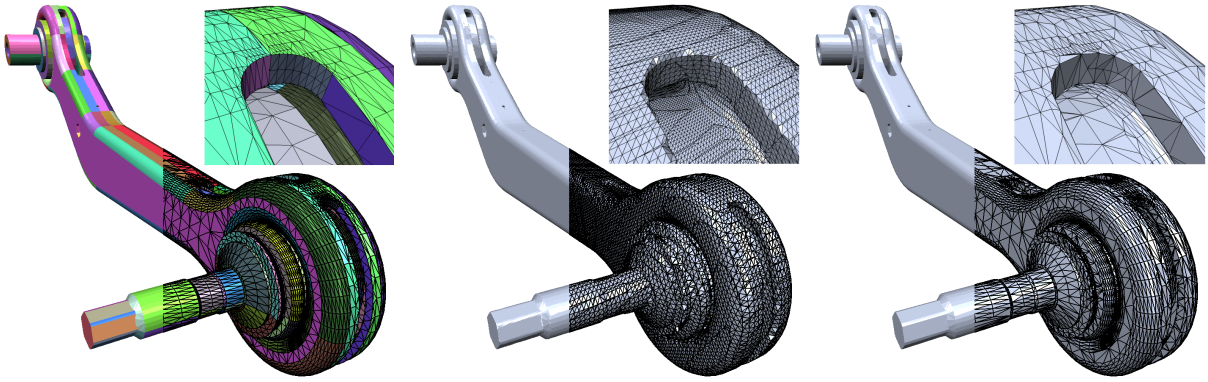

Figure 1: *Our algorithm converts a tessellated CAD model into an intersection-free and closed triangle mesh which covers all gaps up to a prescribed size. Left: The input patches were created by tessellating a CAD model consisting of 385 trimmed NURBS surfaces. Middle: A standard volumetric reconstruction algorithm resamples the model globally and destroys any structure of the tessellation. Right: Our algorithm only resamples the model locally in regions around artifacts like gaps and intersections and thus preserves most of the input tessellation.*

regions that are away from these inconsistencies. We are thus able to preserve any characteristic structure (e.g. iso-parameter or curvature lines) that might be present in the input tessellation. Our algorithm closes gaps up to a user-defined maximum diameter, resolves intersections and overlaps, handles incompatible patch orientations and produces a feature-sensitive, manifold output that stays within a prescribed error-tolerance to the input model.

The basic idea is to first identify the critical regions containing artifacts like gaps and overlaps, then selectively applying a volumetric reconstruction algorithm in these regions and finally joining the reconstruction with the unmodified outside components. Due to its selectivity our algorithm is on the one hand able to achieve high grid resolutions and thus a high reconstruction quality near the artifacts, but on the other hand does not incur the performance overhead of algorithms that globally reconstruct the input.

2. Previous Work

Surface-based algorithms work directly on the input tessellation and use a number of techniques to detect and resolve artifacts. These techniques include, e.g. snapping boundary elements onto each other, projecting and inserting boundary edges into faces, explicitly computing the intersections between faces, propagating the normal field from patch to patch [BW92, BS95, BDK98, GTLH01, MD93], stitching small patches into gaps [TL94, Lie03], resolving topological noise by identifying and cutting handles [GW01], etc.

Surface-based approaches only locally modify the input geometry in a small region around the artifacts. Hence, the input tessellation is preserved wherever possible. However, these approaches usually cannot give any guarantees on the quality of the output: There might be no globally consistent orientation of the input patches; certain artifacts, like overlapping geometry or "double walls" are hard to handle; intersections are difficult to detect and to resolve; due to numerical issues a robust and efficient implementation is challenging.

Volume oriented approaches convert the input into a volumetric representation, i.e. a signed distance field or a grid of directed distances [NT03, Ju04, FPRJ00]. From this volumetric representation one then extracts a surface using techniques like marching cubes [LC87, KBSS01] or dual contouring [Gib98, JLSW02, Ju04].

Volumetric techniques produce guaranteed manifold output. Furthermore, topological artifacts and holes can easily be removed using various filter operations on the volume [ABA02, DMGL02, NT03]. On the downside, however, the conversion to and from a volume acts as a low-pass filter that removes sharp features and leads to aliasing artifacts in the reconstruction. Furthermore, due to the global resampling, the structure of the input patches is completely destroyed and the output is usually highly over-tessellated.

3. Algorithm

The input to our algorithm is a tessellated CAD model $\mathcal{M}_0 = \{\mathcal{P}_1, \ldots, \mathcal{P}_n\}$ which consists of n patches $\mathcal{P}_i$. Each patch $\mathcal{P}_i$ is a manifold triangle mesh and is uniquely identified by its patch ID i. Furthermore, the user prescribes an error tolerance ε_0 and a maximum gap diameter γ_0. The output is an intersection-free and closed triangle mesh $\mathcal{T}$ that approximates $\mathcal{M}_0$ up to a maximum error of ε_0 and covers all gaps of diameter $\leq \gamma_0$. Our algorithm proceeds in several stages (see Figure 2):

1. Conversion of $\mathcal{M}_0$ to a closed mesh $\mathcal{M}$ (Section 3.1)
2. Identification of a set $C \subset \mathbb{Z}^3$ of *critical vertices* that encloses all intersections and all gaps of diameter $\leq \gamma_0$ (Section 3.2)
3. Eroding C to a minimal set C' (Section 3.3)
4. Transforming C' to a set D of *critical cells* that covers all gaps and all intersections (Section 3.4)
5. Clipping $\mathcal{M}$ against D (Section 3.4)
6. Reconstruction of the model geometry inside D (Section 3.5)
7. Postprocessing to reduce the output complexity (Section 3.6)

3.1. Setup

In the following we assume without loss of generality that the input model is scaled and translated such that the error tolerance $\varepsilon_0 = 1$ and that $\mathcal{M}_0$ is enclosed by an integer grid of extent

$$[0,2^k] \times [0,2^k] \times [0,2^k]$$

for some k. Note that the size of the grid cells just equals the error tolerance ε_0. We also assume that the maximum gap diameter is given as $\gamma_0 = 2\gamma$ for some positive integer γ.

We often have to associate data with a small subset of the grid vertices or the grid cells. To improve memory efficiency, this data is stored in the finest-level nodes of an octree of depth k. The octree is adaptively refined on demand, i.e. when we access a certain grid vertex or grid cell.

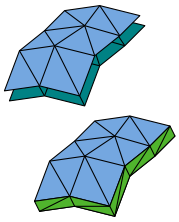

For each patch $\mathcal{P}_i \in \mathcal{M}_0$ we produce a mirror patch $\mathcal{P}_i'$ by duplicating $\mathcal{P}_i$ and reversing the orientation of each triangle. Then we seam $\mathcal{P}_i$ and $\mathcal{P}_i'$ along their common boundary by triangle strips $\mathcal{S}_i$. This yields a new and closed patch $\mathcal{Q}_i$ that represents $\mathcal{P}_i$ from both sides. We collect the new patches in a new model $\mathcal{M} = \{\mathcal{Q}_i\}$. Note that $\mathcal{M}$ is closed, but still contains the same artifacts as $\mathcal{M}_0$. Note also that by this construction our algorithm becomes invariant with respect to the orientation of the input patches. If it turns out that the resulting "double walls" are not necessary to guarantee manifoldness of the reconstruction, they will be removed in the post-processing stage, see Section 3.6.

3.2. Critical regions

In the following we compute a set C_γ of *critical grid vertices*. We think of these critical vertices as particles that fill those regions of space where two or more patches of $\mathcal{M}$ get closer than 2γ. These critical regions include all gaps of diameter $\leq 2\gamma$ and in particular all intersections between different patches. Later stages of the algorithm will then extract the interface between critical vertices and non-critical

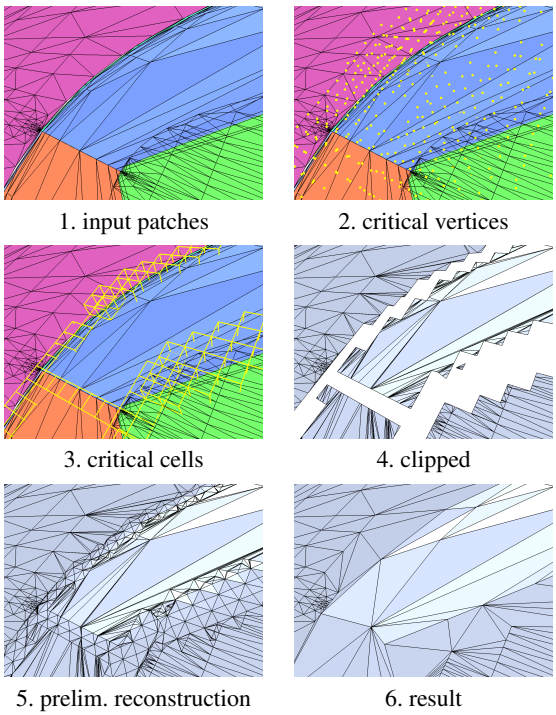

Figure 2: *Stages of our algorithm. The input patches typically exhibit artifacts like gaps and intersections (1). We determine a (rather large) set of critical vertices in a local neighborhood around these artifacts (2) and then convert these vertices into a (smaller) set of critical cells (3). The input patches are clipped against the critical cells (4) and the interior of the cells is reconstructed using a variant of the Marching Cubes algorithm (5). This preliminary reconstruction is then simplified to get the final result (6). Note that the model geometry away from the artifacts is not affected by our reconstruction algorithm and hence any structure in the input patches is well preserved.*

vertices to create surface patches that actually close the gaps and resolve the intersections.

Let us call a grid vertex $\mathbf{v} \in \mathbb{Z}^3$ *ambiguous* if

$$Box_\gamma(\mathbf{v}) := \{\mathbf{w} \in \mathbb{Z}^3 : ||\mathbf{w} - \mathbf{v}||_\infty \leq \gamma\}$$

is intersected by two or more patches of $\mathcal{M}$. If $\mathbf{v}$ is an ambiguous vertex, we set all vertices $\in Box_\gamma(\mathbf{v})$ to *critical*, i.e.

$$C_\gamma := \bigcup_{\mathbf{v}\ \text{ambiguous}} Box_\gamma(\mathbf{v})$$

Figure 3 shows some configurations of $\mathcal{M}$ and the corresponding ambiguous and critical vertices.

Ambiguous vertices can efficiently be located by using a (temporary) octree of depth k. We shift the origin of the octree by $(.5,.5,.5)^T$ such that the centers of the finest-level

octree nodes have integer coordinates, i.e. they correspond to grid vertices. If n is an octree node, we denote by $\mathbf{c}_n \in \mathbb{Z}^3$ its center and by $0 \leq d_n \leq k$ its depth. Hence, if n is a finest-level node ($d_n = k$) we want to check whether

$$Box(n) := Box_\gamma(\mathbf{c}_n)$$

is intersected by two or more different patches. Our idea is to build up a hierarchy of nested boxes which matches the octree hierarchy. Hence, if n is an interior octree node, $Box(n)$ is chosen such that it contains the boxes of all descendants of n. A short calculation shows that this property is fulfilled by letting

$$Box(n) := Box_{h_n}(\mathbf{c}_n), \quad h_n = 2^{k-d_n-1} - 1/2 + \gamma$$

Note in particular, that a triangle intersecting the box of a finest-level node n will also intersect the boxes of all ancestors of n. We now recursively insert each triangle of $\mathcal{M}$ into the octree using an algorithm similar to that of Ju [Ju04]. Starting with the root node, a triangle is inserted into a node n if it intersects $Box(n)$. This can efficiently be tested using the separating axes theorem [GLM96]. If a node n contains triangles belonging to different patches, n is split and the triangles are distributed to its children. In the end, the center $\mathbf{c}_n \in \mathbb{Z}^3$ of each finest-level node n that contains triangles belonging to two or more patches represents an ambiguous vertex.

To increase the resolution of the critical region near $\mathcal{M}$, we also compute the directed distances of each critical vertex $\mathbf{v} \in C_\gamma$ to $\mathcal{M}$ by shooting rays along the coordinate axes (Figure 3). Fortunately, the temporary octree we built up above already provides a spatial search structure to speed up the ray-model intersection tests. If we find an intersection within unit distance, we denote the triple $(\mathbf{v}, \mathbf{d}, \delta)$ consisting of the vertex $\mathbf{v}$, the direction

$$\mathbf{d} \in \pm\{(1,0,0)^T, (0,1,0)^T, (0,0,1)^T\}$$

and the distance $\delta \in [0,1]$ as a *cut*. The cuts will later be used for resampling the geometry at the points $\mathbf{v} + \delta\mathbf{d}$. In the figures, cuts are illustrated as small arrows attached to $\mathbf{v}$ and pointing in direction $\mathbf{d}$, see Figure 3.

3.3. Eroding C_γ

In the previous stage we computed a set $C := C_\gamma$ of critical vertices which we think of as particles that fill in all gaps of $\mathcal{M}$. Later stages of the algorithm will extract the boundary of C to create surface patches that actually close these gaps and resolve the intersections. As this fill-in should alter $\mathcal{M}$ as little as possible, C should be as small as possible. Hence we replace C by a minimal set $C' \subset C$ that still fills in all gaps. We get C' by applying a topology-preserving erosion operator on C, i.e. we successively remove critical vertices from C that are *simple*. (Note that we only remove critical vertices but not the cuts.) Intuitively, a vertex is called simple, if its removal does not change the topology of C, i.e. if it does not create new connected components or handles. The exact definition of simplicity and an efficient method to determine whether a vertex is simple from its 26-neighborhood is given in [BK03]. However, we have to take into account, that in our case the cuts represent material, while in [BK03] the cuts represent empty space.

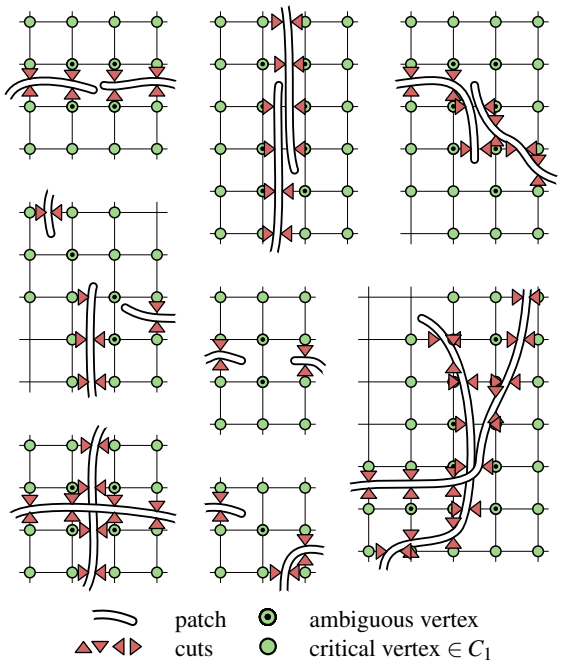

Figure 3: *Example configurations. Some possible configurations of patches $\mathcal{Q} \in \mathcal{M}$ are shown above. Note that each patch is a closed triangle mesh. The critical vertices C_γ fill the regions where two or more different patches of $\mathcal{M}$ are less than 2γ away from each other. Cuts effectively provide sub-voxel accuracy near $\mathcal{M}$.*

We proceed as follows: For each critical vertex $\mathbf{v}$, we compute its distance $d(\mathbf{v})$ to the boundary of C_γ. If $\mathbf{v}$ has a non-critical neighbor, we set $d(\mathbf{v}) = 0$. The distances of the other critical vertices are computed by a distance transform on C_γ that respects the cuts, i.e. distances are not propagated over a cut. We then remove $\lceil 2\gamma \rceil$ layers of simple critical vertices to get a new set C' of critical vertices (Figures 4(left) and 5):

```
for layer=0,1,...,⌈2γ⌉ do
  for all vertices v with d(v)=layer do
    if v is simple then
      set v to non-critical
```

As the following reconstruction will take place along the cuts, there should be cuts between non-critical vertices $\mathbf{w} \notin C'$ and critical vertices $\mathbf{v} \in C'$. Furthermore, there should be no cuts between vertices $\mathbf{v} \in C'$ and $\mathcal{M}$ (Figures 4(right) and 5). Hence, if $\mathbf{v}$ is a critical vertex, we remove all cuts $(\mathbf{v}, \mathbf{d}, \delta)$ and instead insert cuts $(\mathbf{w}, \mathbf{v} - \mathbf{w}, \delta_{smooth})$ for all

non-critical 6-neighbors $\mathbf{w}$ of $\mathbf{v}$. Here, δ_{smooth} is a special value to tell the reconstruction algorithm that $\mathbf{w} + \delta_{smooth}\mathbf{d}$ corresponds to a fill-in and that the corresponding vertices should be smoothed in a postprocessing phase.

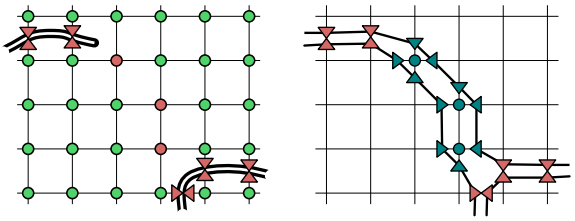

Figure 4: *Erosion. To the left we see the set C_2 of critical vertices that fills in a gap between two patches. The green vertices are removed by a topology-preserving erosion operation. The red vertices cannot be removed without disconnecting the two patches. Right: Each remaining (blue) vertex is replaced by cuts pointing into the vertex. All cuts now form the interface that is extracted in the later stages of the algorithm to close the gaps by surface patches.*

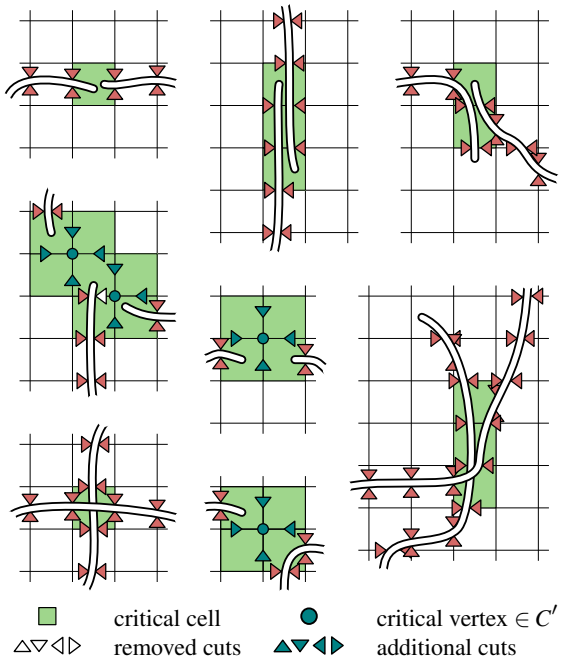

Figure 5: *Example configurations (cont.) The topology-preserving erosion operation (Section 3.3) shrinks C_γ to a smaller set C' which is surrounded by additional cuts. Grid cells that are adjacent to a critical vertex $\in C'$ or that are intersected by multiple patches are marked as critical (Section 3.4).*

3.4. Clipping

In this stage we clip $\mathcal{M}$ against a set of critical grid cells D into an *inside* and an *outside* component such that the inside component contains all the artifacts of the model. The inside component is then discarded and replaced by a well-behaved reconstruction as described in Section 3.5.

First, we need to determine the set of critical grid cells D. As D should cover all artifacts of $\mathcal{M}$, i.e. all intersections and all gaps, we set a grid cell to critical,

- if it contains two or more patches of $\mathcal{M}$ (intersection) *or*
- if one of its incident vertices is critical (gap)

Figure 5 shows some example configurations of $\mathcal{M}$ and their corresponding critical grid cells. In the following, we will denote a grid face as critical, if it shares an un-critical and a critical cell. A grid edge is called critical, if it is incident to a critical face.

The basic idea is to split all triangles of $\mathcal{M}$ along the critical faces into sub-triangles such that each sub-triangle either lies completely inside or completely outside the critical region D. We then simply discard those triangles that lie completely inside.

Although the mathematics of intersecting planar faces is straightforward, the actual implementation of an efficient and numerically robust clipping algorithm is a hard problem. In the following we will present a new algorithm that is specifically tailored to our setup.

- At all times during the run of the algorithm the meshes stay triangle meshes. We do not have to cope with general polygons of arbitrary valence, containing holes, etc. In fact, we modify the meshes using only the Euler-operations *split-1-to-3* and *split-2-to-4 (edge-split)* which are provided as elementary operations by most mesh libraries.
- By using a mixed fixed-point/adaptive-precision representation for the vertex locations, we achieve considerable speedups without sacrifying robustness or accuracy.

The clipping proceeds in three phases which are illustrated in Figure 6. In phase I we intersect the critical edges and the model faces and insert the intersection points into the model using 1-to-3 or 2-to-4 splits. In phase II we intersect the critical faces and the model edges, again inserting the intersection points using 2-to-4 splits. This process automatically produces the edges that result from intersecting a model triangle with all critical grid faces. Thus each triangle now either lies completely inside or completely outside the critical cells. In phase III we then simply discard those triangles whose center of gravity lies in a critical cell.

To effectively enumerate the critical edges and critical faces, we use the recursive octree traversal technique proposed by Ju et al [JLSW02]. However, to speed up the algorithm, before descending into an octree cell, we first test

whether the current triangle really intersects the cell using the separating axis theorem.

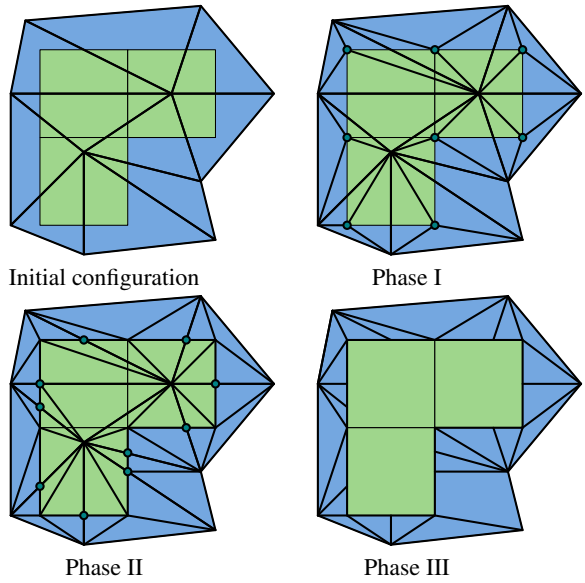

Figure 6: *Initial configuration: A triangle mesh is to be clipped against a set of critical grid cells. Phase I: The intersections of the grid edges with the triangles are inserted into the mesh by 1-to-3-splits or 2-to-4-splits. Phase II: The intersections of mesh edges and grid faces are inserted by 2-to-4-splits. Now each triangle either lies completely inside or completely outside the set of critical grid cells. Phase III: The interior triangles are discarded.*

Implementation The algorithm above only works if intersections are reliably detected and correctly calculated. However, just switching to exact arithmetics will extremely slow down the algorithm. For this reason, we use a mixed representation. Let the positions of the input vertices of the model be quantized to N bits. For each vertex v, we store

- its exact position $\mathbf{p}_{exact,v}$ using an adaptive precision representation [Pri91, She97].
- its approximate position $\mathbf{p}_{approx,v}$ using a fixed point representation of N bits width

such that (remember that the extent of the grid is 2^k):

$$||\mathbf{p}_{exact,v} - \mathbf{p}_{approx,v}|| < \eta := 2^{k-N}$$

We can then use the approximate positions for evaluating "easy rejects" when computing intersection points. Consider for example the intersection of an edge e and a grid face $f = [\mathbf{f}_{min}, \mathbf{f}_{max}]$. We first check whether e_{approx} intersects the box

$$[\mathbf{f}_{min} - (\eta,\eta,\eta)^T, \mathbf{f}_{max} + (\eta,\eta,\eta)^T]$$

This test can exactly be evaluated in fixed-point arithmetics using a maximum of $3N$ bits only [Ju04]. Only if this test is successful, we calculate the real intersection point using exact arithmetics. Analogous considerations apply for triangle-edge intersections, edge-edge intersections, triangle-cell intersections, etc.

3.5. Reconstruction

We now present an algorithm to reconstruct the surface in the interior of the critical cells. This algorithm uses elements of the feature–sensitive marching cubes and dual contouring algorithms that were proposed by Kobbelt et al. [KBSS01] and Ju et al. [JLSW02] and later extended by Varadhan et al. [VKK*03] to arbitrary grids of directed distances. However, in addition to being feature-sensitive, our algorithm can also handle multiple cuts per edge and seamlessly connects the reconstruction inside the critical cells to the outside geometry.

We first enumerate all interior grid faces, again using a recursive octree traversal technique. For each interior grid face, we collect the cuts that are located on the edges of this face. Note that a grid edge might support more than two cuts, if a single patch intersects that edge multiple times. By construction, the number of cuts is always even. Furthermore, cuts pointing in clockwise (cw) direction alternate with cuts pointing in counter-clockwise (ccw) direction. We now connect these cuts by edges: a cw cut is connected to the next ccw cut by going ccw around the grid face (Figure 7, left), see also [Blo88, NH91]. If we connect two cuts from the same grid edge, we insert an auxiliary point at the face center to prevent topological degeneracies. Note that by construction, the edges do not intersect.

We then visit each critical cell in turn. The edges on the cell's faces were either created as described above or are boundary edges of the outside geometry. In any case, these edges form one or more connected loops around the cell. Each of these loops is triangulated by a triangle fan (Figure 7, right). As the edges do not intersect, the loops will also be free of intersections and so are the triangle fans.

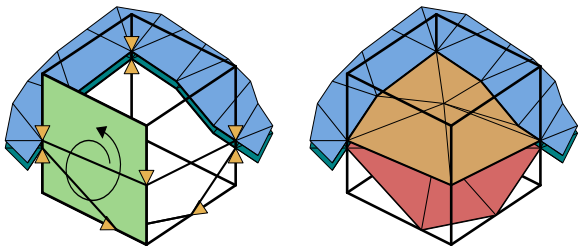

Figure 7: *We connect the cuts incident to a grid face by edges (left). For each grid cell these edges and the boundary edges of the outside geometry form loops around the cell. Each of these loops is triangulated by a fan of triangles (right).*

The position **p** of the fan's center vertex is computed by minimizing the squared distances to the supporting planes of the triangles that intersect the grid cell [Lin00]. Note that, if the cell contains a feature edge or corner, this construction will place **p** exactly on the feature. If the computed point **p** happens to lie outside the cell or if it does not lie on all supporting planes, it is set to *invalid*. Invalid vertices are smoothed in the post-processing stage. Finally we flip the edges in interior grid faces, such that the center vertices become connected. This guarantees feature vertices in neighboring cells to be connected by a (feature) edge (Figure 8).

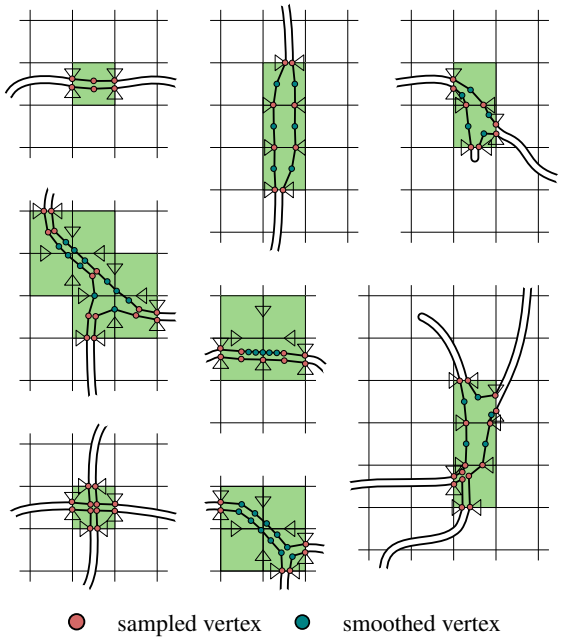

Figure 8: *Example configurations (cont.) The geometry in the critical grid cells is replaced by a reconstructed surface $\mathcal{R}$ which is extracted from the cuts using a variant of the Marching Cubes algorithm. Some of the vertices of $\mathcal{R}$ can directly be sampled from $\mathcal{M}$. Others, however, correspond to those parts of $\mathcal{R}$ that cover the gaps of $\mathcal{M}$. The position of these vertices is determined by an iterative smoothing filter.*

3.6. Postprocessing

Smoothing After the reconstruction stage the positions of the following types of vertices is not yet determined.

- Vertices that correspond to those parts of the reconstruction that span gaps of $\mathcal{M}$ and hence have no canonical position. These are the vertices that either are derived from cuts $(\mathbf{v}, \mathbf{d}, \delta_{smooth})$ or are the centers of triangle fans that are created in an empty grid cell.
- Vertices that are the centers of triangle fans in grid cells that contain conflicting geometry — usually due to an insufficient refinement depth k.

In both cases we smooth the vertex positions by applying an iterative smoothing filter [Tau95].

Decimation The output of the reconstruction algorithm is a closed and manifold triangle mesh $\mathcal{T}$ which approximates the input model $\mathcal{M}$ but has all artifacts resolved. However, $\mathcal{T}$ usually contains much more vertices and faces than $\mathcal{M}_0$ due to the artificial refinement near the gaps. This can be attributed to two effects

- Every patch of the input model is represented from both sides by $\mathcal{T}$.
- The higher the resolution of the underlying grid, the more triangles are needed for reconstructing the model in the critical regions.

Accordingly, we have two options for reducing the output complexity. First, the mesh $\mathcal{T}$ usually consists of multiple connected components, only few of which really contribute to the outside of $\mathcal{M}$. The other components merely triangulate $\mathcal{M}$ from the inside and hence can be easily identified and discarded. The identification can be done manually or automatically by a flood fill process as in [Ju04]. Second, we apply a standard feature-sensitive mesh decimation algorithm to $\mathcal{T}$ [GH97]. However, to preserve the input tessellation of $\mathcal{M}$, we only do this in regions that were reconstructed anyway.

4. Results

We have evaluated our method on a number of CAD models of different complexities (Figures 9, 10, 11). All timings were taken on a 2GB, 3.2 GHz Pentium 4 computer.

Choice of input parameters As our algorithm only reconstructs the regions around artifacts and as this local reconstruction is further decimated in the postprocessing phase, the output complexity grows typically only sub-linearly with respect to the grid resolution. Hence we can use high grid resolutions to improve the reconstruction quality without incuring an undue overhead of generated triangles. If the tessellation of the input patches is sufficiently accurate, we can set $\gamma = 1$ without missing any gaps even for high resolutions.

Asymptotic behaviour If the artifacts form a one dimensional subspace e.g. along the intersection of two surfaces or along two abutting patches, the number of critical vertices and cells should in theory grow linearly with respect to the grid resolution for a constant γ. Our experimental results match well with this theoretical statement, only the Camera model (Figure 10) is an exception because it contains a lot of interior geometry and "double walls". These artifacts cannot suffiently be resolved and hence the critical vertices and cells actually form a two or three-dimensional subspace. In these regions the octree has to be refined to maximum depth, which causes a significant increase in memory usage.

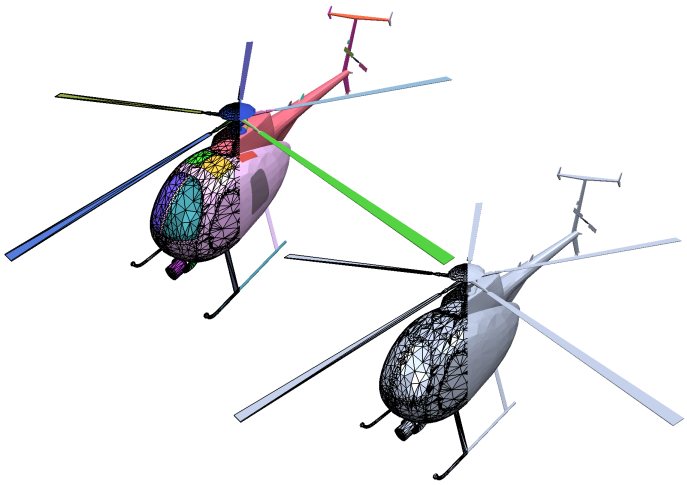

Helicopter, 10 k triangles in 60 patches, $\gamma = 1$				
resolution	1024^3	2048^3	4096^3	8192^3
#critical vertices	242 k	505 k	1037 k	2079 k
#critical cells	68 k	141 k	277 k	561 k
#output triangles	28 k	34 k	44 k	60 k
time	47 s	116 s	291 s	868 s

Figure 9: *Helicopter*

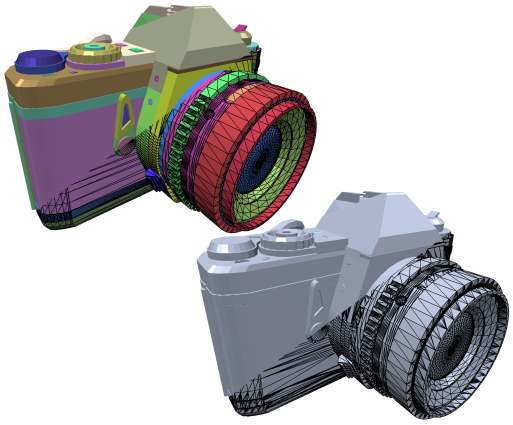

Camera, 19 k triangles in 83 patches, $\gamma = 1$			
resolution	128^3	256^3	512^3
#critical vertices	192 k	655 k	1978 k
#critical cells	83 k	270 k	874 k
#output triangles	33 k	61 k	81 k
time	56 s	145 s	639 s

Figure 10: *Camera*

5. Discussion

We have presented a new and efficient algorithm for fully automatic and selective repair of tessellated CAD models. However, a number of issues are still open for future work.

Artifacts within a single patch Our algorithm does reliably detect and resolve artifacts between different patches. However, it does not resolve artifacts within a single patch, like e.g. self-intersections. Of course, we could extend our algorithm to also handle such artifacts, but that would significantly decrease its performance. The reason is, that during the construction of the vertex octree, we often have to check whether a certain box contains two or more patches. Currently this check is very fast, as we only have to compare the patch IDs of the participating triangles. However, if we also wanted to detect self-intersections within a single patch, we would actually have to intersect each triangle with all other triangles in the box. This can be done very fast [SAUK04] but as none of our models has self-intersecting patches, we conclude that such a situation does not happen very often in practice. If it does, the user has to manually divide the patch into non-self-intersecting subpatches.

Selectivity Our algorithm does only modify critical regions of the model, i.e. regions containing intersections or gaps, and preserves the structure of the tessellation everywhere else. These critical regions are determined fully automatically from a global user-defined parameter γ_0. It should, however, be possible to let this parameter locally depend on the underlying model geometry such as to close gaps of different sizes. It should also be possible to apply one of the surface oriented mesh repair algorithms in a preprocessing step to segment the input into large and manifold patches wherever possible and apply our method only to those regions where the surface oriented methods fail.

Reconstruction We reconstruct the surface in the critical regions from a grid of directed distances using a novel contouring algorithm. This algorithm correctly resolves any self-intersections based on the local configuration of the cuts around a grid face only. However, other (possibly global) criteria might also be incorporated. For example, we might strive for a reconstruction of minimal genus or of minimal number of connected components. For a standard grid of signed distances and the Marching Cubes algorithm, this has already been explored by Andujar et al. [ABC*04].

Space and time efficiency Due to its selectivity, our algorithm already proved to be quite space and time efficient. In our implementation we have used standard libraries for the octree and mesh data structures and for the exact arithmetic and the mesh decimation framework. We believe that we could achieve considerable speed ups and lower memory usage if we used custom-tailored data structures and algorithms instead. As our algorithm operates on local information only, it should also be easily possible to generalize it to parallel machines.

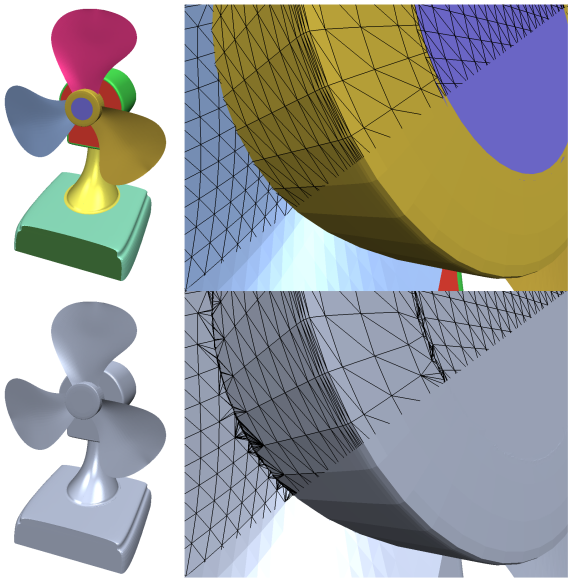

Ventilator, 269 k triangles in 12 patches, $\gamma = 2$				
resolution	1024^3	2048^3	4096^3	8192^3
#critical vertices	238 k	460 k	828 k	1649 k
#critical cells	64 k	113 k	229 k	523 k
#output triangles	503 k	512 k	529 k	556 k
time	83 s	123 s	193 s	303 s

Figure 11: *Ventilator*

References

[ABA02] ANDUJAR C., BRUNET P., AYALA D.: Topology-reducing surface simplification using a discrete solid representation. *ACM Trans. Graph. 21*, 2 (2002), 88–105.

[ABC*04] ANDUJAR C., BRUNET P., CHICA A., NAVAZO I., ROSSIGNAC J., VINACUA A.: Optimizing the topological and combinatorial complexity of isosurfaces. *Computer-Aided Design to appear* (2004).

[BDK98] BAREQUET G., DUNCAN C., KUMAR S.: RSVP: A geometric toolkit for controlled repair of solid models. *IEEE Trans. on Visualization and Computer Graphics 4*, 2 (1998), 162–177.

[BK03] BISCHOFF S., KOBBELT L.: Sub-voxel topology control for level-set surfaces. *Computer Graphics Forum 22*, 3 (September 2003), 273–280.

[Blo88] BLOOMENTHAL J.: Polygonization of implicit surfaces. *Computer Aided Geometric Design 5*, 4 (1988), 341–355.

[BS95] BAREQUET G., SHARIR M.: Filling gaps in the boundary of a polyhedron. *Computer-Aided Geometric Design 12*, 2 (1995), 207–229.

[BW92] BØHN J. H., WOZNY M. J.: Automatic CAD model repair: Shell-closure. In *Proc. Symp. on Solid Freeform Fabrication* (1992), pp. 86–94.

[DMGL02] DAVIS J., MARSCHNER S., GARR M., LEVOY M.: Filling holes in complex surfaces using volumetric diffusion. In *Proc. International Symposium on 3D Data Processing, Visualization, Transmission* (2002), pp. 428–438.

[FPRJ00] FRISKEN S. F., PERRY R. N., ROCKWOOD A. P., JONES T. R.: Adaptively sampled distance fields: A general representation of shape for computer graphics. In *Proc. SIGGRAPH 00* (2000), pp. 249–254.

[GH97] GARLAND M., HECKBERT P. S.: Surface simplification using quadric error metrics. In *Proc. SIGGRAPH 97* (1997), pp. 209–216.

[Gib98] GIBSON S. F. F.: Using distance maps for accurate surface representation in sampled volumes. In *Proc. IEEE Symposium on Volume Visualization* (1998), pp. 23–30.

[GLM96] GOTTSCHALK S., LIN M. C., MANOCHA D.: OBBTree: a hierarchical structure for rapid interference detection. In *Proc. SIGGRAPH 96* (1996), pp. 171–180.

[GTLH01] GUÉZIEC A., TAUBIN G., LAZARUS F., HORN B.: Cutting and stitching: Converting sets of polygons to manifold surfaces. *IEEE Transactions on Visualization and Computer Graphics 7*, 2 (2001), 136–151.

[GW01] GUSKOV I., WOOD Z. J.: Topological noise removal. In *Proc. Graphics Interface 2001* (2001), pp. 19–26.

[JLSW02] JU T., LOSASSO F., SCHAEFER S., WARREN J.: Dual contouring of hermite data. In *Proc. SIGGRAPH 02* (2002), pp. 339–346.

[Ju04] JU T.: Robust repair of polygonal models. In *Proc. SIGGRAPH 04* (2004), pp. 888–895.

[KBSS01] KOBBELT L. P., BOTSCH M., SCHWANECKE U., SEIDEL H.-P.: Feature sensitive surface extraction from volume data. In *Proc. SIGGRAPH 01* (2001), pp. 57–66.

[LC87] LORENSEN W. E., CLINE H. E.: Marching cubes: A high resolution 3D surface construction algorithm. In *Proc. SIGGRAPH 87* (1987), pp. 163–169.

[Lie03] LIEPA P.: Filling holes in meshes. In *Proc. Symposium on Geometry Processing 03* (2003), pp. 200–205.

[Lin00] LINDSTROM P.: Out-of-core simplification of large polygonal models. In *Proc. SIGGRAPH 02* (2000), pp. 259–262.

[MD93] MÄKELÄ I., DOLENC A.: Some efficient procedures for correcting triangulated models. In *Solid Freeform Fabrication Symposium Proceedings* (1993), pp. 126–134.

[NH91] NIELSON G. M., HAMANN B.: The asymptotic decider: resolving the ambiguity in marching cubes. In

VIS '91: Proceedings of the 2nd conference on Visualization '91 (1991), pp. 83–91.

[NT03] NOORUDDIN F., TURK G.: Simplification and repair of polygonal models using volumetric techniques. *IEEE Transactions on Visualization and Computer Graphics 9*, 2 (2003), 191–205.

[Pri91] PRIEST D. M.: Algorithms for arbitrary precision floating point arithmetic. In *Tenth Symposium on Computer arithmetic* (1991), pp. 132–143.

[SAUK04] SHIUE L.-J., ALLIEZ P., URSU R., KETTNER L.: *A Tutorial on CGAL Polyhedron for Subdivision Algorithms*. Tech. rep., 2004.

[She97] SHEWCHUK J. R.: Adaptive precision floating-point arithmetic and fast robust geometric predicates. *Discrete & Computational Geometry 18* (1997), 305–363.

[Tau95] TAUBIN G.: A signal processing approach to fair surface design. In *Proc. SIGGRAPH 95* (1995), pp. 351–358.

[TL94] TURK G., LEVOY M.: Zippered polygon meshes from range images. In *Proc. SIGGRAPH 94* (1994), pp. 311–318.

[VKK*03] VARADHAN G., KRISHNAN S., KIM Y., DIGGAVI S., MANOCHA D.: Efficient max-norm distance computation and reliable voxelization. In *Proc. Symposium on Geometry Processing* (2003), pp. 116–126.